



Platinum nanoparticles decorated multiwalled carbon nanotube composites as highly transparent, bifacial counter electrodes for dye-sensitized solar cells

R. Krishnapriya¹ · C. Nizamudeen¹ · A.-H. I. Mourad^{1,2,3}

Received: 7 September 2023 / Accepted: 13 November 2023 / Published online: 28 November 2023
© The Author(s) 2023

Abstract

Dye-sensitized solar cells (DSSCs) are low-cost solar energy conversion devices with variable color and transparency advantages. DSSCs' potential power efficiency output, even in diffuse light conditions with consistent performance, allows them to be used in building-integrated photovoltaics (BIPV) window applications. Significantly, the development of bifacial DSSCs is getting significant scientific consideration. Triiodide/iodide (I_3^-/I^-) redox couple-mediated DSSCs require highly effective and stable electrocatalysts for I_3^- reduction to overcome their performance constraints. However, the commonly employed platinum (Pt) cathodes have restrictions on high price and unfavorable durability. Here, we report platinum nanoparticles (Pt NPs) incorporated into multiwalled carbon nanotubes (MWCNT) composites with lower Pt content as an efficient bifacial counter electrode (CE) material for DSSC applications. Pt NPs were homogeneously decorated over the MWCNT surfaces using a simple polyol method at relatively low temperatures. CEs fabricated using Pt/MWCNT composites exhibited excellent transparency and power conversion efficiencies (PCE) of 6.92% and 6.09% for front and rear illumination. The results are expected to bring significant advances in bifacial DSSCs for real-world window applications.

Keywords Transparent electrode · Solvothermal · Platinum · Multiwalled carbon nanotubes · Dye-sensitized solar cells

Introduction

Low-cost and energy-efficient solar energy conversion technology to reduce electricity costs is the most significant challenge of this century. Among the other well-established solar cells, dye-sensitized solar cells (DSSCs) stand out as

a potential candidate owing to their high energy conversion efficiency, efficient work in diffuse light, and ease of fabrication protocols [1, 2]. A typical DSSC functions upon the interface interaction of the anode, electrolyte, and counter electrode (CE). On illumination, a nanostructured dye-coated TiO_2 photo anode produces photo-injected electrons, which are then transferred to an iodide/triiodide (I^-/I_3^-) redox couple electrolyte. A subsequent generation of the redox couple occurs at the metal CE [3–6]. The CE has essential effects on the photovoltaic parameters of DSSCs. An effective CE should have strong electrocatalytic activity and excellent conductivity to reduce the redox couple.

Till now, noble metal platinum (Pt) has been the most successfully employed and efficient CE in DSSCs due to its corrosion resistance and exceptional electrocatalytic activity toward the I^-/I_3^- redox couple [7]. However, Pt NPs' high price and tendency to aggregate frequently prompt material scientists to look at viable substitutes. Counter electrodes based on carbon, conducting polymers, transition metal sulfides, reduced graphene oxide, and composites are often employed as CEs [8–10]. However, the electrodes' catalytic

R. Krishnapriya and C. Nizamudeen have contributed equally to this work.

A.-H. I. Mourad was on leave from Mechanical Design Department, Faculty of Engineering, Helwan University, Cairo, Egypt during the time of this work.

✉ A.-H. I. Mourad
ahmourad@uaeu.ac.ae

¹ Mechanical and Aerospace Engineering Department, College of Engineering, United Arab Emirates University, 15551 Al Ain, United Arab Emirates

² National Water and Energy Centre, United Arab Emirates University, 15551 Al Ain, United Arab Emirates

³ Mechanical Design Department, Faculty of Engineering, Helwan University, Cairo, Egypt

activity and stability obtained were not as excellent as nano-Pt [11–13].

Dropping the quantity of catalyst Pt and dispersing the catalyst homogeneously over a suitable, cost-effective catalytic support are the two strategic ways to minimize the DSSC manufacturing costs instead of sacrificing the electrocatalytic performance. Several studies on transition metal oxides, acetylene black, carbon black, etc., were reported in the literature as competent support materials for Pt [14–17]. Notably, low Pt-containing composites with diverse supporting materials are a viable class of CE material for DSSC and are currently gaining considerable attention [18–20]. In this regard, multi-walled carbon nanotubes (MWCNTs) are a highly promising supporting material as they are chemically stable and have favorable electrical and thermal conductivity [21–25]. Moreover, the functionalized MWCNTs can nicely disperse and hold various metal NPs firmly over their surface with the advantage of having a large surface area [26].

In addition to the scientific advancement to find a substitute for Pt CEs with low-cost materials, high transparency should be considered for real-world window applications. In recent years, considerable progress has been made in developing solution-processed transparent electrodes (TEs) for DSSC applications [27–29]. Faster throughput and reduced energy requirements make solution-processed TEs cost-effective in solar cells [30]. Additionally, the technique permits the homogeneous deposition of electrode materials with strong adhesion and remarkable mechanical resilience on flexible and even curved surfaces. Because of their transparent electrodes, these bifacial DSSCs can produce up to 50% more electrical energy than conventional DSSCs [31–34]. TEs fabricated using various polymers are strong candidates for low-cost bifacial DSSCs [35–39]. However, the thermal stability of these polymeric electrodes limits their commercial application. Therefore, the fabrication of TEs utilizing thermally stable materials is crucial.

In this context, this work aims to explore the use of the MWCNT application for transparent DSSCs by hybridizing it with Pt NPs. A simple polyol method synthesized Pt/MWCNT catalysts. The synthesis of composites was carried out at relatively low temperatures. The MWCNT with highly dispersed Pt NPs was spin-coated over a fluorine-doped tin oxide (FTO) glass to obtain highly transparent CEs. The material characterization and DSSC device performance were analyzed via front and back illumination.

Materials

All the chemical reactants such as hexachloroplatinic acid (~40% Pt, CAS No 18497-13-7), ethylene glycol (99.8%) MWCNTs (>95%, CAS No. 308068-56-6), HNO₃ (70%, CAS No. 7697-37-2) and H₂SO₄ (95–98%, CAS No.

7664-93-9) were purchased from Sigma Aldrich, used as received without further purification.

Functionalization of MWCNTs

The acid functionalization of the MWCNT was carried out to introduce functional groups (–COOH, –CHO, –CO) on the surface using a mixture of concentrated acids. For this, 0.05 g of MWCNT was added to 40 mL of acid solution (Containing 3:1 of H₂SO₄ and HNO₃) followed by continuous stirring of contents for 24 h. The precipitate was washed three times with deionized water and then dried.

Synthesis of Pt/MWCNT composite

A simple solvothermal method prepared Pt-MWCNT composite by the in-situ reduction of chloroplatinic acid with ethylene glycol (EG) as the solvent. During the solvothermal reaction, EG acts as a mild reducing agent to get Pt⁰. The chelating effect of EG avoids the agglomeration of Pt NPs on the surface of MWCNT. In a typical procedure, 0.036 g of acid-functionalized MWCNT was dispersed into 40 mL of ethylene glycol by sonication of the mixture for 15 min. To this 0.05/0.1/0.15 g H₂PtCl₆ was added, and the whole solution was subjected to a solvothermal reaction for 6 h at 180 °C. The precipitate obtained is washed with acetone several times and dried in air for further characterization. The obtained sample weighed 0.078 g, 0.126 g, and 0.177 g, respectively.

Fabrication of DSSCs

The DSSCs and their components were fabricated using the method described in previous works [40]. At first, photoanodes were prepared on cleaned FTO glass. A homogeneous viscous paste of pristine TiO₂ with 2 mL ethanol and 1–2 drops of Triton[®] X-100 was doctor-blade into the FTO glass with an active area of 0.25 cm². The substrate is then heated at 450 °C for 1 h to obtain a transparent photoanode layer with an approximate film thickness of 10 ± 5 μm. The photoanode was cooled below 80 °C for dye loading and kept in 0.5 mM N719 dye for 12 h. The Pt counter electrode was prepared by drop casting one drop H₂PtCl₆ solution (~0.05 mL, 0.001 g Pt) into FTO glass and heating them in a furnace at 400 °C for 20 min. To compare the CE performance, the Pt/MWCNT composites synthesized using 0.05 g Pt precursor were used to fabricate cells. The composite is dispersed in 2 mL of isopropanol solution and sonicated for 5 min. From the obtained homogeneous solution, ~0.05 mL (0.0006 g Pt and 0.0004 g MWCNT) of the solution is drop-casted onto the cleaned FTO and dried in a vacuum oven for 100 for 2 h. The fabricated photoanode and counter electrode sandwiched together using a surlyn

film spacer with a thickness of 30 μm to fabricate the cell. One or two drops of redox couple electrolyte consisting of 0.06 M 1-butyl-3-methyl imidazolium iodide, 0.03 M of iodine (I₂), 0.10 M guanidinium thiocyanate, 0.5 M 4-tert-butylpyridine was prepared in a mixed solvent containing acetonitrile and valeronitrile in 85:15 (volume ratio) was injected into DSSCs using a glass syringe prior to photovoltaic measurements.

Characterization

The crystal phase identification of all the samples was inspected using a high-resolution X-ray diffractometer (RIGAKU, ULTIMA IV, JAPAN) with Cu K α radiation ($\lambda = 1.54 \text{ \AA}$) at 40 kV and 30 mA. The phase was compared with standard ICDD (International Centre for Diffraction Data). The surface morphology of the samples was perceived by a field emission scanning electron microscope (FESEM-SUPRA-55-Carlzeiss, Germany). Raman spectroscopic analysis was carried out using a confocal Raman microscope (RENISHAW, UNITED KINGDOM) using a semiconductor diode laser of excitation energy 514 nm.

Three DSSC devices made of identical samples were fabricated for PV measurements for each case. The current–voltage (J – V) measurements were executed under simulated light of power 100 mWcm^{-2} with Newport® 150 W 96000 solar simulator using AM1.5 Global filter. Prior to the J – V characterization, the light intensity of the xenon lamp was calibrated using a standard silicon photodiode. The J – V data were recorded using a Keithley 2400 source meter at RT in the air. CV and EIS measurements were done using a potentiostat–galvanostat instrument (Biologic-SP-150).

Results and discussion

The Pt/MWCNT composites were prepared via acid functionalization of MWNT followed by glycothermal reduction of H_2PtCl_6 and MWCNT mixture. The schematics of the whole synthesis process are given in Scheme 1.

The adopted polyol synthesis methodology is a versatile and low-cost route for synthesizing various metals, alloys, and metal oxides, where ethylene glycol is used as

the solvent. The EG solvent can simultaneously serve as a solvent, stabilizer, and reducing agent, limiting the Pt particle growth and preventing agglomeration [41, 42]. The Pt/MWCNT composites prepared after washing and drying are used to further characterize and fabricate CEs. Figure 1 shows the powder XRD pattern of the synthesized Pt/MWCNT nanocomposite and MWCNT. Diffraction peaks obtained were matched with the standard ICDD data of Platinum and graphite (platinum: 87–0647 and graphite: 75–1621). For MWCNT, characteristic graphitic carbon peaks observed at 25.9 and 43.4 corresponds to (002) and (100) planes [43]. For the Pt/MWCNT composite, the (002) peak intensity was reduced (enlarged spectra), and characteristic peaks (111), (200), and (220) of the face-centered cubic (fcc) structure of platinum were observed [44, 45]. No oxidized Pt peaks were observed. This specifies the successful formation of Pt-MWCNT composite. The average particle size of Pt was calculated using Scherrer's equation is 7 nm. No other impurity peaks were observed, revealing the completion of the reaction and the purity of the as-prepared composite.

The morphologic features of the samples were analyzed using the FESEM analysis. Figure 2 shows the low

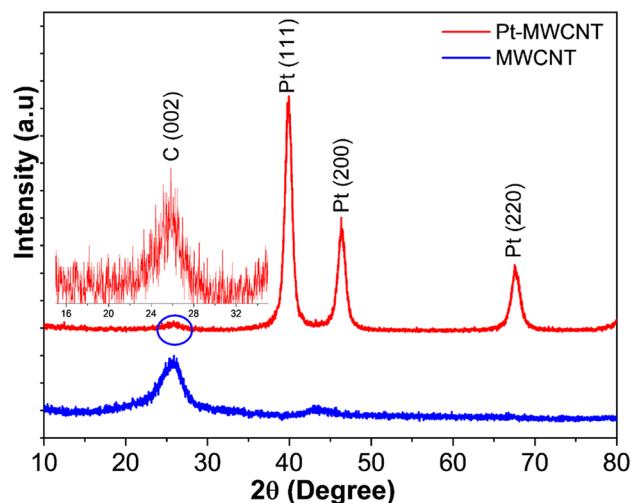


Fig. 1 Powder XRD patterns of the MWCNT and Pt/MWCNT composites prepared by glycothermal reduction

Scheme 1 Schematics of synthesis of Pt/MWCNT composites using a facile glycothermal process

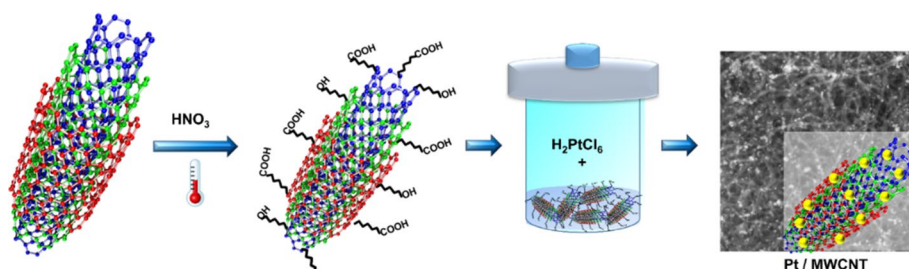


Fig. 2 The low and high-magnification FESEM images of Pt/MWCNT composite sample

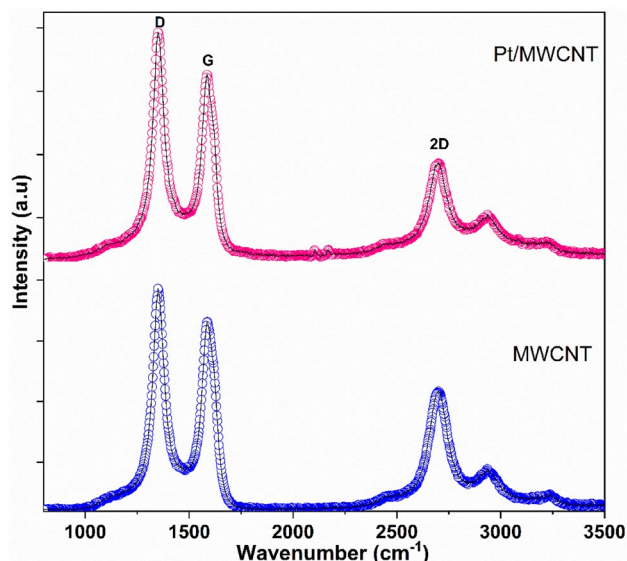
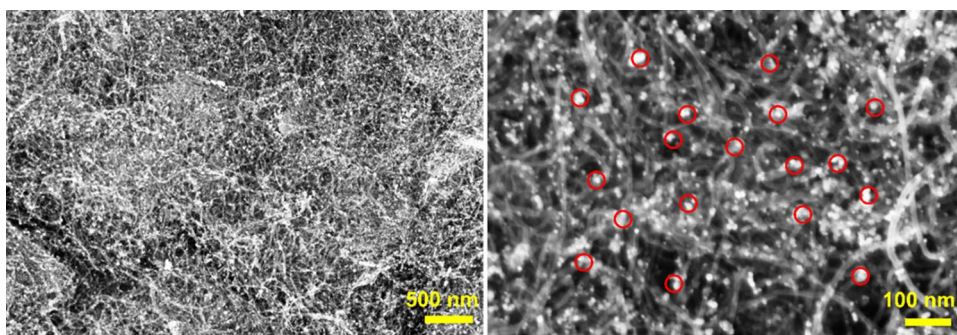


Fig. 3 The Raman spectra of the MWCNT and Pt/MWCNT composites

and high-magnification FESEM images of the prepared Pt-MWCNT nanocomposite. The fiber-like morphological features of MWCNTs were maintained after incorporating Pt nanoparticles, as evident in the SEM image. From Fig. 3c, Pt NPs are visible as light dots spread over the surface layers of MWCNT. Also, the Pt NPs (red circle) were found to be decorated all over the surface of MWCNT. The surface of MWCNT acts as an adequate support to hold the Pt NPs [46]. This unique hybrid structure is beneficial for providing strong catalytic sites with a good electron conduction pathway [43].

The Raman spectroscopy examination (Fig. 3) provided further details regarding the phase and purity of the substance. The two prominent peaks at 1564 and 1334 cm^{-1} correspond to the G-band and the D-band of CNTs [47]. The existence of impurities and structural flows or disorders were linked to the D-band at around 1334 cm^{-1} . The -band at 1564 cm^{-1} denotes the E2g stretching vibration of HCP carbon atom [48]. The ID/IG ratio represents the

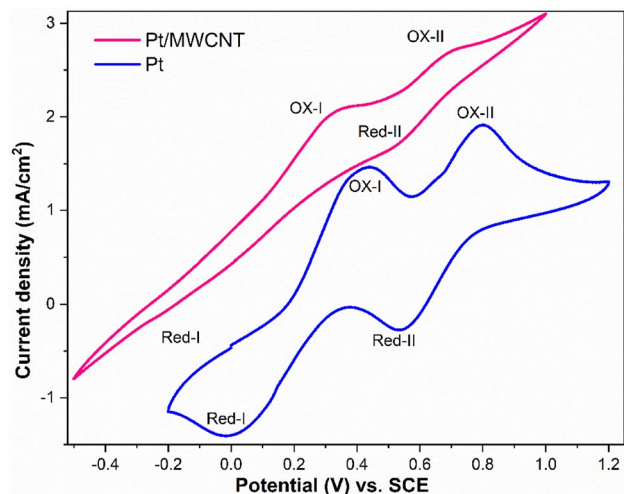


Fig. 4 The CV spectra of fabricated CEs with Pt and Pt/MWCNT composites recorded at a scan rate of 50 mV s^{-1}

defect caused in CNT during chemical processing [49]. The insertion of functional groups on the surface, which causes structural deformations, results in a greater (ID/IG) ratio for the functionalized MWCNTs (0.94), compared to the non-functionalized MWCNTs (0.67). These findings are consistent with those in the literature.

Using a three-electrode setup with Ag/AgCl as the reference electrode and Pt wire as the CE with a scan rate of 50 mV s^{-1} , the electrocatalytic performance of CEs made using Pt/MWCNT and Pt was examined. The samples were drop cast for preparing the working electrode. The electrolyte consisted of 10 mM LiI, 1 mM I_2 and 0.1 M LiClO_4 in acetonitrile. Both samples showed two pairs of redox peaks in the CV, as seen in Fig. 4. The oxidation and reduction of I^-/I_3^- were attributed to the negative redox pair (Ox-I and Red-I), while I_2/I_3^- was given to the positive redox pair (Ox-II and Red-II), as shown by the equations below:





Analyzing the negative redox pair of the Pt/MWCNT samples is crucial since the CE in DSSCs is responsible for the catalytic reduction of I_3^- to I^- . Peak currents and peak separation, which are two distinctive metrics, may be used to assess the catalytic activity of the manufactured CE (Epp). According to an estimation made using the following equation, the peak-to-peak separation (Epp) is inversely proportional to the rate constant of a redox reaction:

$$E_{pp} = |E_p(\text{anodic}) - E_p(\text{cathodic})|$$

Two sets of redox peaks were observed corresponding to the I^-/I_3^- redox couple (Ox-I/Red-I) and I_3^-/I_2^- (Ox-II/Red-II) in both the CEs employed. The peak-to-peak potential separation between the redox peaks (Ox-I/Red-I) for Pt is 0.43 mV, while for the Pt/MWCNT it is reduced by 0.41 mV. This indicates a more facile reduction of the I^- species taking place on the Pt/MWCNT. The increased peak current for the oxidation of I^- (in the first redox pair) and I_3^- (second redox pair) also suggests to the increased oxidation of the iodine species on the Pt/MWCNT compared to the Pt. However, the difference between the oxidation peak currents and the reduction peak currents is lower in the Pt-MWCNTs compared to Pt. This may suggest an irreversibility of the

redox pairs in the Pt-MWCNT compared to the Pt. Though agreeably, the MWCNTs do provide an enhanced surface area for the I^-/I_3^- redox couple, the redox kinetics could be hampered by the inaccessibility of the electrolyte solution inside the MWCNTs [50, 51].

Figure 5 shows the photocurrent–voltage (J – V) characteristic curves for the DSSCs employing best-performing Pt/MWCNT CEs. The measurements were conducted under standard AM 1.5G conditions with a 100 mW/cm² light intensity. To understand the performance under front-illumination and back-illumination conditions, 0.25 cm² cell area-based DSSCs were made. The extracted photovoltaic parameters from the J – V characteristic curves are presented in Table 1.

It is evident that the bare Pt CE exhibited a better electrical conductivity than the Pt/MWCNTs CE and showed maximum PCE (7.97%) and J_{sc} (15.62 mA/cm²) among all the fabricated CEs with FF of 0.71. However, the front-illuminated Pt/MWCNT composites-based DSSCs showed significant PCE (6.92%) with remarkable current (13.9 mA/cm²), voltage (0.73 V), and FF (0.68). The V_{oc} of CEs fabricated using Pt/MWCNT composites is higher than Pt implying better adhesion of the prepared CE material to the FTO surface. The FF values show that the Pt/MWCNT CE with back illumination shows less recombination loss.

The charge-transfer characteristics of the cells were studied using electrochemical impedance spectroscopy (EIS). EIS analysis was carried out using dummy cells fabricated in a symmetric cell configuration with Pt/MWCNT CEs. Figure 6 demonstrates the Nyquist plots of CEs. The inset presents the equivalent circuit for the perfect fit of plots to obtain the charge transport and transfer parameters inside the cells. The semicircle obtained denotes charge transfer resistance (R_{ct}). The lowest R_{ct} was related to a quicker charge-transfer kinetics, which could be due to the larger electrocatalytically active area of CE. It was observed that Pt/MWCNT CEs exhibited higher R_{ct} values, resulting in reduced catalytic activity. Compared to Pt/MWCNT nano-hybrid CEs, Pt exhibited much lower R_{ct} , indicating higher catalytic activity. Thus, EIS studies demonstrated the effective charge transfer at the redox electrolyte/MWCNT CE interface, resulting in enhanced electrocatalytic performance of Pt toward the electrolyte reduction reaction. The composite samples showed 6.92% PCE on front illumination and 6.09% on back illumination. There is only 12% efficiency

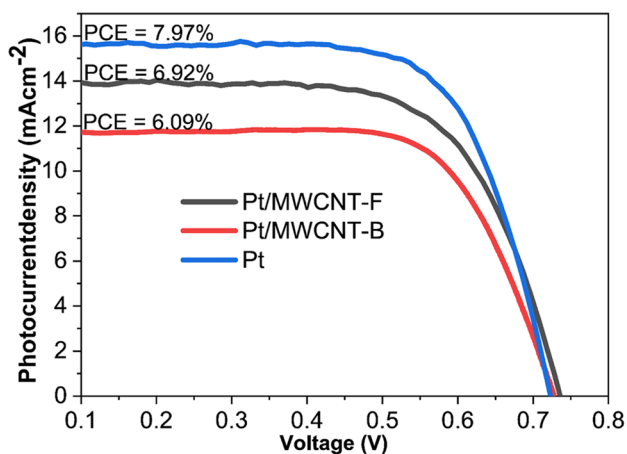


Fig. 5 The J – V characteristic curves for the fabricated DSSCs using the Pt and Pt/MWCNT composites

Table 1 The PV parameters extracted from the J – V characterization curve

Cell	J_{sc} (mA/cm ²)	V_{oc} (V)	J_{max} (mA/cm ²)	V_{max} (V)	FF	PCE (%)
Pt/MWCNT-F	13.9	0.73	12.37	0.55	0.68	6.92
Pt/MWCNT-B	11.71	0.72	10.99	0.55	0.72	6.09
Pt	15.62	0.71	14.30	0.55	0.71	7.97

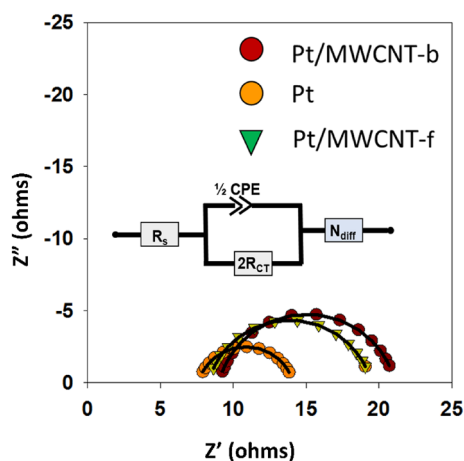


Fig. 6 Comparative impedance spectra of Pt/MWCNT CE with the inset representing the equivalent circuit used to fit the impedance spectra

loss compared to front illumination. The data obtained were corroborated with the EIS studies.

The stability test for the fabricated cells was carried out under ambient conditions for 20 days, and the PV data extracted are given in Table 2. The cells exhibited very little loss in PV parameters. Hence, the composite CEs

demonstrated can be applied for highly efficient stable DSSCs.

The promising PV performance of the devices is due to the high transparency of the CEs. The MWCNT content in the composite can provide a high surface area that can uniformly distribute the Pt NPs over its surface [52, 53]. Moreover, the high transparency of the CE can provide better LHE and reduced internal recombination loss and acts as an efficient electrocatalyst, as obtained from EIS studies [54, 55]. Such bifacial DSSCs are very beneficial for commercializing DSSCs as window panels. Table 3 provides the comparative PV performance of DSSCs fabricated using different composite CEs using MWCNT.

From Table 3, it can be understood that the fabricated Pt/MWCNT-based CEs are very promising in terms of delivering good PCEs. ZnCo₂S₄@MWCNT and SrCo₂S₄@f-MWCNTs@N-RGO CEs showed high performance compared to Pt/MWCNT CEs. However, the synthesis process adopted for the study was complex with respect to the polyol method reported in this study. Hence, it is believed that the current work will throw some light on the better and ultimate usage of Pt/MWCNT as CEs in DSSCs and other solar cells. We further studied the cost effectiveness of the DSSCs using Pt/MWCNT. The amount of Pt used to fabricate the pristine Pt electrode using one

Table 2 Stabilities of the best-performing DSSCs studied over 20 days under ambient conditions

Cell	PCE				V _{oc}			
	0 days	5 days	10 days	20 days	0 days	5 days	10 days	20 days
Pt/MWCNT-F	6.92	6.77	6.69	6.57	0.73	0.73	0.72	0.72
Pt/MWCNT-B	6.09	5.96	5.88	5.78	0.72	0.72	0.72	0.71
Pt	7.97	7.73	7.63	7.49	0.71	0.71	0.70	0.70
	J _{sc}				FF			
Pt/MWCNT-F	13.9	13.83	13.76	13.62	0.68	0.67	0.66	0.66
Pt/MWCNT-B	11.71	11.65	11.59	11.48	0.72	0.71	0.71	0.71
Pt	15.62	15.54	15.46	15.31	0.71	0.70	0.69	0.69

Table 3 Comparative PV performance of DSSCs fabricated using MWCNT-based counter electrodes

References	Materials	V _{OC} V	J _{SC} mA cm ⁻²	FF	η/%
[56]	ZnCo ₂ S ₄ @MWCNT	0.74	17.99	0.65	8.55
[57]	NiCo ₂ S ₄ /MWCNT	0.71	9.02	0.55	4.14
[58]	SrCo ₂ S ₄ @f-MWCNTs@N-RGO	0.74	16.32	0.70	8.06
[59]	MWCNT-NixSn ₂ xS ₄ x	0.71	10.85	0.60	4.67
[60]	f-MWCNT@NiMOSe ₂	0.70	19.93	0.53	7.39
[61]	MoS ₂ / MWCNTs	0.36	2.41	0.64	0.55
[62]	MWCNT	0.75	11.67	0.57	5.01
[63]	Sb ₂ S ₃ @ MWCNT	0.68	12.70	0.49	5.00
This work	Pt/MWCNT-F	0.73	13.90	0.68	6.92

drop of composite was calculated as 0.001 g, while for the Pt/MWCNT electrode, it was 0.0006 g Pt and 0.0004 g MWCNT. Thus, the amount of Pt used per cell was reduced almost by half. Furthermore, the market price of Pt is more than double that of MWCNT, the approach has resulted in a 25% reduction in the cost of the counter electrode per unit cell. This reduction significantly contributes to lowering the overall cost of the solar cell.

Conclusion

The Pt/MWCNT composites were prepared by a simple one-pot polyol method. The crystal planes of both Pt and MWCNT observed in XRD which confirm the successful formation of Pt/MWCNT composites. Highly dispersed Pt NPs over the MWCNT surfaces were identified with SEM analysis. Raman spectroscopic techniques further confirmed phase purity of the MWCNT. Homogeneously anchored Pt NPs, over MWCNTs, were drop cast on FTO to get highly transparent CEs that can be used as bifacial CEs for DSSCs. The fabricated electrodes demonstrated the best cell efficiencies, such as 6.92% and 6.09%, respectively, for the front and rear-illuminated DSSCs. The promising PV parameters obtained are J_{sc} (13.9 mA/cm²), V_{oc} (0.73 V), and FF (0.68) for front illumination. Whereas back-illuminated DSSCs showed J_{sc} (11.71 mA/cm²), V_{oc} (0.72 V), and FF (0.72), respectively. The obtained PCE results from the highly conductive and transparent nature of the composite CEs. The polyol synthesis adopted facilitated the homogeneous distribution and strong adhesion of Pt NPs over the MWCNT surfaces. The catalytic activity of the Pt NPs decorated MWCNT was characterized by CV measurements and showed lower R_{ct} and higher peak current for I_3^- reduction. From the study, it is revealed that the cost of the counter electrode per unit cell has decreased by 25%. Consequently, using MWCNT is anticipated to significantly reduce the cost of DSSC without sacrificing PCE for large-scale production.

Funding This study was funded by grant 31R238 from UAE University, Al Ain, United Arab Emirates.

Data availability The data supporting this study's findings are available from the corresponding author upon request.

Declarations

Conflict of interest The authors declare that they have no known competing financial interests or personal relationships that could have appeared to influence the work reported in this paper.

Open Access This article is licensed under a Creative Commons Attribution 4.0 International License, which permits use, sharing, adaptation, distribution and reproduction in any medium or format, as long as you give appropriate credit to the original author(s) and the source,

provide a link to the Creative Commons licence, and indicate if changes were made. The images or other third party material in this article are included in the article's Creative Commons licence, unless indicated otherwise in a credit line to the material. If material is not included in the article's Creative Commons licence and your intended use is not permitted by statutory regulation or exceeds the permitted use, you will need to obtain permission directly from the copyright holder. To view a copy of this licence, visit <http://creativecommons.org/licenses/by/4.0/>.

References

- Muñoz-García, A.B., Benesper, I., Boschloo, G., Concepcion, J.J., Delcamp, J.H., Gibson, E.A., Meyer, G.J., Pavone, M., Pettersson, H., Hagfeldt, A., Freitag, M.: Dye-sensitized solar cells strike back. *Chem. Soc. Rev.* **50**(22), 12450–12550 (2021). <https://doi.org/10.1039/D0CS01336F>
- Santos, F., Ivanou, D., Mendes, A.: The renaissance of monolithic dye-sensitized solar cells. *Mater. Today Commun.* **32**, 104030 (2022). <https://doi.org/10.1016/j.mtcomm.2022.104030>
- Agrawal, A., Siddiqui, S.A., Soni, A., Sharma, G.D.: Advancements, frontiers and analysis of metal oxide semiconductor, dye, electrolyte and counter electrode of dye sensitized solar cell. *Sol. Energy* **233**, 378–407 (2022). <https://doi.org/10.1016/j.solener.2022.01.027>
- Nizamudeen, C., Krishnapriya, R., Mozumder, M., Mourad, A.I., Ramachandran, T.: Photovoltaic performance of MOF-derived transition metal doped titania-based photoanodes for DSSCs. *Sci. Rep.* **13**(1), 6345 (2023)
- Krishnapriya, R., Nizamudeen, C., Saini, B., Mozumder, M.S., Sharma, R.K., Mourad, A.H.I.: MOF-derived Co²⁺-doped TiO₂ nanoparticles as photoanodes for dye-sensitized solar cells. *Sci. Rep.* **11**(1), 16265 (2021). <https://doi.org/10.1038/s41598-021-95844-4>
- Cherupurakal, N., Ramachandran, K.P., Mourad, A.H.I.: Enhancing the performance of dye-sensitized solar cells by Co²⁺ doping in MOF derived TiO₂. In: 2022 Advances in Science and Engineering Technology International Conferences (ASET), pp 1–5. (2022). <https://doi.org/10.1109/ASET53988.2022.9734951>
- Wu, J., Lan, Z., Lin, J., Huang, M., Huang, Y., Fan, L., Luo, G., Lin, Y., Xie, Y., Wei, Y.: Counter electrodes in dye-sensitized solar cells. *Chem. Soc. Rev.* **46**(19), 5975–6023 (2017)
- Ahmad, K., Mohammad, A., Mobin, S.M.: Hydrothermally grown α -MnO₂ nanorods as highly efficient low cost counter-electrode material for dye-sensitized solar cells and electrochemical sensing applications. *Electrochim. Acta.* **252**, 549–557 (2017). <https://doi.org/10.1016/j.electacta.2017.09.010>
- Ahmad, K., Shinde, M.A., Song, G., Kim, H.: Design and fabrication of MoSe₂/WO₃ thin films for the construction of electrochromic devices on indium tin oxide based glass and flexible substrates. *Ceram. Int.* **47**(24), 34297–34306 (2021). <https://doi.org/10.1016/j.ceramint.2021.08.340>
- Ahmad, K., Shinde, M.A., Kim, H.: Molybdenum disulfide/reduced graphene oxide: progress in synthesis and electro-catalytic properties for electrochemical sensing and dye sensitized solar cells. *Microchem. J.* **169**, 106583 (2021). <https://doi.org/10.1016/j.microc.2021.106583>
- Shahzad, N., Lutfullah, P.T., Pugliese, D., Haq, S., Fatima, N., Salman, S.M., Tagliaferro, A., Shahzad, M.I.: Counter electrode materials based on carbon nanotubes for dye-sensitized solar cells. *Renew. Sustain. Energy Rev.* **159**, 112196 (2022). <https://doi.org/10.1016/j.rser.2022.112196>
- Tapa, A.R., Xiang, W., Zhao, X.: Metal chalcogenides (M x E y; E = S, Se, and Te) as counter electrodes for dye-sensitized

- solar cells: an overview and guidelines. *Adv. Energy Sustain. Res.* **2**(10), 2100056 (2021). <https://doi.org/10.1002/aesr.202100056>
13. Kladkaew, M., Lin, J.-Y., Chanlek, N., Vailikhit, V., Hasin, P.: Well-dispersive polypyrrole and MoSe₂ embedded in multiwalled carbon nanotube@reduced graphene oxide nanoribbon electrocatalysts as the efficient counter electrodes in rigid and plastic dye-sensitized solar cells. *ACS Appl. Energy Mater.* (2022). <https://doi.org/10.1021/acsaem.2c03305>
 14. Ahmad, W., Chu, L., Al-bahrani, M.R., Ren, X., Su, J., Gao, Y.: P-type NiO nanoparticles enhanced acetylene black as efficient counter electrode for dye-sensitized solar cells. *Mater. Res. Bull.* **67**, 185–190 (2015). <https://doi.org/10.1016/j.materresbull.2015.03.021>
 15. Liu, I.P., Hou, Y.-C., Li, C.-W., Lee, Y.-L.: Highly electrocatalytic counter electrodes based on carbon black for cobalt(iii)/(ii)-mediated dye-sensitized solar cells. *J. Mater. Chem. A* **5**(1), 240–249 (2017). <https://doi.org/10.1039/C6TA08818J>
 16. Wu, K., Wu, Y., Fu, P., Yang, D., Ruan, B., Wu, M., Wu, R.: Composites of vanadium (III) oxide (V₂O₃) incorporating with amorphous C as Pt-free counter electrodes for low-cost and high-performance dye-sensitized solar cells. *ACS Omega* **6**(17), 11183–11191 (2021). <https://doi.org/10.1021/acsomega.0c05880>
 17. Don, M.F., Ekanayake, P., Nakajima, H., Mahadi, A.H., Lim, C.M.: Improvement of dye-sensitized solar cell performance through introducing TiO₂ in acetylene carbon black-graphite composite electrode. *Thin Solid Films* **706**, 138042 (2020). <https://doi.org/10.1016/j.tsf.2020.138042>
 18. Ghifari, A., Long, D.X., Kim, S., Ma, B., Hong, J.: Transparent platinum counter electrode prepared by polyol reduction for bifacial, dye-sensitized solar cells. *Nanomaterials* **10**(3), 502 (2020)
 19. Poudel, P., Zhang, L., Joshi, P., Venkatesan, S., Fong, H., Qiao, Q.: Enhanced performance in dye-sensitized solar cells via carbon nanofibers–platinum composite counter electrodes. *Nanoscale* **4**(15), 4726–4730 (2012). <https://doi.org/10.1039/C2NR30586K>
 20. Poudel, P., Thapa, A., Elbohy, H., Qiao, Q.: Improved performance of dye solar cells using nanocarbon as support for platinum nanoparticles in counter electrode. *Nano Energy* **5**, 116–121 (2014). <https://doi.org/10.1016/j.nanoen.2014.02.003>
 21. Lee, W.J., Ramasamy, E., Lee, D.Y., Song, J.S.: Efficient dye-sensitized solar cells with catalytic multiwall carbon nanotube counter electrodes. *ACS Appl. Mater. Interfaces* **1**(6), 1145–1149 (2009). <https://doi.org/10.1021/am800249k>
 22. Jeon, I., Xiang, R., Shawky, A., Matsuo, Y., Maruyama, S.: Single-walled carbon nanotubes in emerging solar cells: synthesis and electrode applications. *Adv. Energy Mater.* **9**(23), 1801312 (2019). <https://doi.org/10.1002/aenm.201801312>
 23. Jeon, I., Yoon, J., Kim, U., Lee, C., Xiang, R., Shawky, A., Xi, J., Byeon, J., Lee, H.M., Choi, M., Maruyama, S., Matsuo, Y.: High-performance solution-processed double-walled carbon nanotube transparent electrode for perovskite solar cells. *Adv. Energy Mater.* **9**(27), 1901204 (2019). <https://doi.org/10.1002/aenm.201901204>
 24. Mohammadnezhad, M., Selopal, G.S., Wang, Z.M., Stansfield, B., Zhao, H., Rosei, F.: Role of carbon nanotubes to enhance the long-term stability of dye-sensitized solar cells. *ACS Photonics* **7**(3), 653–664 (2020). <https://doi.org/10.1021/acsp Photonics.9b01431>
 25. Mohammadnezhad, M., Selopal, G.S., Cavuslar, O., Barba, D., Durmusoglu, E.G., Acar, H.Y., Wang, Z.M., Lopinski, G.P., Stansfield, B., Zhao, H., Rosei, F.: Gold nanoparticle decorated carbon nanotube nanocomposite for dye-sensitized solar cell performance and stability enhancement. *Chem. Eng. J.* **421**, 127756 (2021). <https://doi.org/10.1016/j.cej.2020.127756>
 26. Sun, Y.-P., Fu, K., Lin, Y., Huang, W.: Functionalized carbon nanotubes: properties and applications. *Acc. Chem. Res.* **35**(12), 1096–1104 (2002). <https://doi.org/10.1021/ar010160v>
 27. Zhang, Y., Ng, S.-W., Lu, X., Zheng, Z.: Solution-processed transparent electrodes for emerging thin-film solar cells. *Chem. Rev.* **120**(4), 2049–2122 (2020). <https://doi.org/10.1021/acs.chemrev.9b00483>
 28. Tai, Q., Yan, F.: Emerging semitransparent solar cells: materials and device design. *Adv. Mater.* **29**(34), 1700192 (2017). <https://doi.org/10.1002/adma.201700192>
 29. Mozumder, M.S., Mourad, A.-H.I., Pervez, H., Surkatti, R.: Recent developments in multifunctional coatings for solar panel applications: a review. *Sol. Energy Mater. Sol. Cells* **189**, 75–102 (2019). <https://doi.org/10.1016/j.solmat.2018.09.015>
 30. Cai, H., Tang, Q., He, B., Li, R., Yu, L.: Bifacial dye-sensitized solar cells with enhanced rear efficiency and power output. *Nanoscale* **6**(24), 15127–15133 (2014). <https://doi.org/10.1039/C4NR04911J>
 31. Saifullah, M., Gwak, J., Yun, J.H.: Comprehensive review on material requirements, present status, and future prospects for building-integrated semitransparent photovoltaics (BISTPV). *J. Mater. Chem. A* **4**(22), 8512–8540 (2016). <https://doi.org/10.1039/C6TA01016D>
 32. Venkatesan, S., Lin, W.-H., Teng, H., Lee, Y.-L.: High-Efficiency bifacial dye-sensitized solar cells for application under indoor light conditions. *ACS Appl. Mater. Interfaces* **11**(45), 42780–42789 (2019). <https://doi.org/10.1021/acsaami.9b14876>
 33. Sasidharan, S., Pradhan, S.C., Jagadeesh, A., Nair, B.N., Mohamed, A.A.P., KN, N.U., Soman, S., Hareesh, U.N.S.: Bifacial dye-sensitized solar cells with enhanced light scattering and improved power conversion efficiency under full sun and indoor light conditions. *ACS Appl. Energy Mater.* **3**(12), 12584–12595 (2020). <https://doi.org/10.1021/acsaem.0c02500>
 34. Venkatesan, S., Cho, Y.-S., Liu, I.-P., Teng, H., Lee, Y.-L.: Novel architecture of indoor bifacial dye-sensitized solar cells with efficiencies surpassing 25% and efficiency ratios exceeding 95%. *Adv. Opt. Mater.* **9**(22), 2100936 (2021). <https://doi.org/10.1002/adom.202100936>
 35. Wu, J., Li, Y., Tang, Q., Yue, G., Lin, J., Huang, M., Meng, L.: Bifacial dye-sensitized solar cells: a strategy to enhance overall efficiency based on transparent polyaniline electrode. *Sci. Rep.* **4**(1), 4028 (2014). <https://doi.org/10.1038/srep04028>
 36. Ahn, S., Jeong, S.-H., Han, T.-H., Lee, T.-W.: Conducting polymers as anode buffer materials in organic and perovskite optoelectronics. *Adv. Opt. Mater.* **5**(3), 1600512 (2017). <https://doi.org/10.1002/adom.201600512>
 37. Yao, X., He, B., Cui, L., Ti, J., Chen, H., Duan, Y., Tang, Q.: Polypyrrole-molybdenum sulfide complex as an efficient and transparent catalytic electrode for bifacial dye-sensitized solar cells. *Catal. Commun.* **163**, 106403 (2022). <https://doi.org/10.1016/j.catcom.2022.106403>
 38. Zhu, T., Yang, Y., Yao, X., Huang, Z., Liu, L., Hu, W., Gong, X.: Solution-processed polymeric thin film as the transparent electrode for flexible perovskite solar cells. *ACS Appl. Mater. Interfaces* **12**(13), 15456–15463 (2020). <https://doi.org/10.1021/acsaami.9b22891>
 39. Cherupurakal, N., Mozumder, M.S., Mourad, A.-H.I., Lalwani, S.: Recent advances in superhydrophobic polymers for antireflective self-cleaning solar panels. *Renew. Sustain. Energy Rev.* **151**, 111538 (2021). <https://doi.org/10.1016/j.rser.2021.111538>
 40. Krishnapriya, R., Praneetha, S., Rabel, A.M., Vadivel Murugan, A.: Energy efficient, one-step microwave-solvothermal synthesis of a highly electro-catalytic thiospinel NiCo₂S₄/graphene nano-hybrid as a novel sustainable counter electrode material for Pt-free dye-sensitized solar cells. *J. Mater. Chem. C* **5**(12), 3146–3155 (2017). <https://doi.org/10.1039/C6TC04619C>
 41. Sun, Y., Xia, Y.: Shape-controlled synthesis of gold and silver nanoparticles. *Science* **298**(5601), 2176–2179 (2002). <https://doi.org/10.1126/science.1077229>

42. Herricks, T., Chen, J., Xia, Y.: Polyol synthesis of platinum nanoparticles: control of morphology with sodium nitrate. *Nano Lett.* **4**(12), 2367–2371 (2004). <https://doi.org/10.1021/nl048570a>
43. Yao, Y., Izumi, R., Tsuda, T., Oshima, Y., Imanishi, A., Oda, N., Kuwabata, S.: Platinum and PtNi nanoparticle-supported multiwalled carbon nanotube electrocatalysts prepared by one-pot pyrolytic synthesis with an ionic liquid. *ACS Appl. Energy Mater.* **2**(7), 4865–4872 (2019). <https://doi.org/10.1021/acsaem.9b00561>
44. Bonet, F., Delmas, V., Grugeon, S., Herrera Urbina, R., Silvert, P.Y., Tekaiia-Elhissen, K.: Synthesis of monodisperse Au, Pt, Pd, Ru and Ir nanoparticles in ethylene glycol. *Nanostruct. Mater.* **11**(8), 1277–1284 (1999). [https://doi.org/10.1016/S0965-9773\(99\)00419-5](https://doi.org/10.1016/S0965-9773(99)00419-5)
45. Tong, H., Li, H.-L., Zhang, X.-G.: Ultrasonic synthesis of highly dispersed Pt nanoparticles supported on MWCNTs and their electrocatalytic activity towards methanol oxidation. *Carbon* **45**(12), 2424–2432 (2007). <https://doi.org/10.1016/j.carbon.2007.06.028>
46. Yang, X.H., Guo, J.W., Yang, S., Hou, Y., Zhang, B., Yang, H.G.: A free radical assisted strategy for preparing ultra-small Pt decorated CNTs as a highly efficient counter electrode for dye-sensitized solar cells. *J. Mater. Chem. A* **2**(3), 614–619 (2014). <https://doi.org/10.1039/C3TA13986G>
47. Dresselhaus, M.S., Dresselhaus, G., Saito, R., Jorio, A.: Raman spectroscopy of carbon nanotubes. *Phys. Rep.* **409**(2), 47–99 (2005)
48. Wang, H.-Y., Wang, F.-M., Wang, Y.-Y., Wan, C.-C., Hwang, B.-J., Santhanam, R., Rick, J.: Electrochemical formation of Pt nanoparticles on multiwalled carbon nanotubes: useful for fabricating electrodes for use in dye-sensitized solar cells. *J. Phys. Chem. C* **115**(16), 8439–8446 (2011). <https://doi.org/10.1021/jp201220t>
49. Lehman, J.H., Terrones, M., Mansfield, E., Hurst, K.E., Meunier, V.: Evaluating the characteristics of multiwall carbon nanotubes. *Carbon* **49**(8), 2581–2602 (2011). <https://doi.org/10.1016/j.carbon.2011.03.028>
50. Park, J.T., Lee, C.S., Kim, J.H.: High performance electrocatalyst consisting of CoS nanoparticles on an organized mesoporous SnO₂ film: its use as a counter electrode for Pt-free, dye-sensitized solar cells. *Nanoscale* **7**(2), 670–678 (2015). <https://doi.org/10.1039/C4NR05779A>
51. Guo, J.W., Zhang, B., Hou, Y., Yang, S., Yang, X.H., Yang, H.G.: A sulfur-assisted strategy to decorate MWCNTs with highly dispersed Pt nanoparticles for counter electrode in dye-sensitized solar cells. *J. Mater. Chem. A* **1**(6), 1982–1986 (2013). <https://doi.org/10.1039/C2TA01003H>
52. Wu, M., Sun, M., Zhou, H., Ma, J.-Y., Ma, T.: Carbon counter electrodes in dye-sensitized and perovskite solar cells. *Adv. Func. Mater.* **30**(7), 1906451 (2020). <https://doi.org/10.1002/adfm.201906451>
53. Yu, F., Shi, Y., Yao, W., Han, S., Ma, J.: A new breakthrough for graphene/carbon nanotubes as counter electrodes of dye-sensitized solar cells with up to a 10.69% power conversion efficiency. *J. Power. Sources* **412**, 366–373 (2019). <https://doi.org/10.1016/j.jpowsour.2018.11.066>
54. Shahid, M.U., Mohamed, N.M., Muhsan, A.S., Bashiri, R., Shamsudin, A.E., Zaine, S.N.A.: Few-layer graphene supported polyaniline (PANI) film as a transparent counter electrode for dye-sensitized solar cells. *Diam. Relat. Mater.* **94**, 242–251 (2019). <https://doi.org/10.1016/j.diamond.2019.03.009>
55. Peng, J.-D., Wu, Y.-T., Yeh, M.-H., Kuo, F.-Y., Vittal, R., Ho, K.-C.: Transparent cobalt selenide/graphene counter electrode for efficient dye-sensitized solar cells with Co²⁺/3⁺-based redox couple. *ACS Appl. Mater. Interfaces* **12**(40), 44597–44607 (2020). <https://doi.org/10.1021/acsami.0c08220>
56. Baptyayev, B., Tashenov, Y., Adilov, S., Balanay, M.P.: Facile fabrication of ZnCo₂S₄@MWCNT as Pt-free counter electrode for high performance dye-sensitized solar cells. *Surf. Interfaces* **37**, 102699 (2023)
57. Gayathri, V., John Peter, I., Ramachandran, K., Karazhanov, S., Raja Mohan, C.: Graphene quantum dots embedded in NiCo₂S₄/MWCNT nanocomposite as a promising candidate for supercapacitors and I₃⁻ reduction in dye-sensitized solar cells. *Energy Fuels* **35**(16), 13360–13369 (2021)
58. Zhang, W., Khan, M.W., Zuo, X., Yang, Q., Tang, H., Jin, S., Li, G.: Sunflower-Like SrCo₂S₄@f-MWCNTs hybrid wrapped by engineering N-reduced graphene oxide for high performance dye-sensitized solar cells. *J. Renew. Mater.* **8**(4), 431 (2020)
59. Saravanakumar, T., Selvaraju, T., Bhojanaa, K., Ramesh, M., Pandikumar, A., Akilan, R., Shankar, R., Basha, S.S.: Exploring the synergistic effect of Ni x Sn 2x S 4x thiospinel with MWCNTs for enhanced performance in dye-sensitized solar cells, the hydrogen evolution reaction, and supercapacitors. *Dalton Trans.* **49**(16), 5336–5351 (2020)
60. Mirzaei, M., Gholivand, M.B.: Introduction of Pt-free counter electrode based on f-MWCNTs@NiMoSe₂ nanocomposite for efficient dye-sensitized solar cells. *Sol. Energy* **227**, 67–77 (2021)
61. Mithari, P.A., Mendhe, A.C., Karade, S.S., Sankapal, B.R., Patrikar, S.R.: MoS₂ nanoflakes anchored MWCNTs: counter electrode in dye-sensitized solar cell. *Inorg. Chem. Commun.* **132**, 108827 (2021)
62. Younas, M., Gondal, M., Dastageer, M., Baig, U.: Fabrication of cost effective and efficient dye sensitized solar cells with WO₃-TiO₂ nanocomposites as photoanode and MWCNT as Pt-free counter electrode. *Ceram. Int.* **45**(1), 936–947 (2019)
63. Peter, I.J., Vijaya, S., Anandan, S., Nithiananthi, P.: Sb₂S₃ entrenched MWCNT composite as a low-cost Pt-free counter electrode for dye-sensitized solar cell and a viewpoint for a photo-powered energy system. *Electrochim. Acta.* **390**, 138864 (2021)

Publisher's Note Springer Nature remains neutral with regard to jurisdictional claims in published maps and institutional affiliations.